Thermal properties of knotted block copolymer rings with charged monomers subjected to short-range interactions

Neda Abbasi Taklimi [1,*] Franco Ferrari [1,†] Marcin Radosław Piątek [1,‡] and Luca Tubiana [2,3,§]

[1] *CASA* and Institute of Physics, University of Szczecin, 70-453 Szczecin, Poland*
[2] *Physics Department, University of Trento, I-38123 Trento, Italy*
[3] *INFN-TIFPA, Trento Institute for Fundamental Physics and Applications, I-38123 Trento, Italy*

The thermal properties of coarse-grained knotted copolymer rings fluctuating in a highly screening solution are investigated on a simple cubic lattice using the Wang-Landau Monte Carlo algorithm. The rings contain two kinds of monomers A and B with opposite charges that are subjected to short-range interactions. In view of possible applications in medicine and the construction of intelligent materials, it is shown that the behavior of copolymer rings can be tuned by changing both their monomer configuration and topology. We find several phase transitions depending on the monomer distribution. They include the expansion and collapse of the knotted polymer as well as rearrangements leading to metastable states. The temperatures at which these phase transitions are occurring and other features can be tuned by changing the topology of the system. The processes underlying the observed transitions are identified. In knots formed by diblock copolymers, two different classes of behaviors are detected depending on whether there is an excess of monomers of one kind or not. Moreover, we find that the most stable compact states are formed by copolymers in which units of two A monomers are alternated by units of two B monomers. Remarkably, these compact states are in a lamellar phase. The transition from the lamellar to the expanded state produces in the specific heat capacity a narrow and high peak that is centered at temperatures that are much higher than those of the peaks observed in all other monomer distributions.

I. INTRODUCTION

Polymer knots are abundant in nature and in artificial polymeric materials [1–5]. They can be created in the laboratory [4–6] and have attracted considerable attention both from experimentalists and theoreticians working in several different disciplines including chemistry [7–9], engineering [10,11], mathematics [12,13], and physics [14–23]. We consider here the static properties of knots made by copolymer rings containing two different kinds of charged monomers A and B in an ion solution. Our investigations are conducted using the Wang-Landau Monte Carlo algorithm [24]. The main advantage of the algorithm is that, once the density of states is computed, it gives a complete overview of the thermal properties of the systems under consideration over the whole range of temperatures. It is also very efficient in sampling rare events, which play an important role in the low temperature range.

Part of the motivations of this work come from biology. In fact, DNA and other biomolecules are characterized by regions that have different properties and can thus be regarded as copolymers. Recently, a diblock copolymer approximation of a piece of DNA has been used in order to understand how the dishomogeneities in the flexibility affect the localization of

knots on a piece of circular DNA [25,26]. Knotted copolymer rings can be useful also in technological applications. For instance, it is already known that the presence of knots affects the behavior of polymer materials. Indeed, the elastic response of elastomers cannot be understood without considering the fact that the polymer chains inside these materials form knots and links [27]. The effects of the presence of knots on the conformational properties of AB diblock-copolymer rings have already been noted for instance in Ref. [28].

The statistical mechanics of open or circular copolymers has been investigated in the past, see, e.g., Refs. [29–35]. Systems similar to those treated here have been considered in Refs. [36–38] and, more recently, in Refs. [39,40]. There has been also some interest on circular diblock copolymers with nontrivial topologies [25,26,28,39,41–44]. For example, in Ref. [39] it has been shown how the stiffness heterogeneity or the presence of charges influence the localization of the knot. The role of stiffness and heterogeneity in knot production has been explored in Ref. [45]. Other aspects of topology in copolymers have been treated in Ref. [44]. Some more general systems have been considered in relation to specific aspects, like for instance the knotted hydrophobic-polar (HP) models in proteins [46,47] and the self-assembly of nanomaterials of specific topologies controlled by tuning the properties of patchy heteropolymers [19]. Previous studies of the statistical mechanics of knotted homopolymers and copolymers with the help of the Wang-Landau algorithm [24] can be found for example in Refs. [48,49] (homopolymers) and Refs. [37,50] (copolymers).

*neda.abbasi_taklimi@phd.usz.edu.pl
†franco@feynman.fiz.univ.szczecin.pl
‡marcin.piatek@usz.edu.pl
§luca.tubiana@unitn.it

In this paper we extend the earlier results in the subject by providing an extensive survey considering several knot topologies and many different monomer configurations. It emerges from our investigations that knotted copolymer rings enjoy remarkable properties depending on the monomer distribution including the presence of intermediate phases and a lamellar phase. While the relevant parameters of a polymer knot, like gyration radius, heights and temperatures of the peaks of the heat capacity, specific energy, and number of contacts (noncontiguous monomers that are at the distance of one lattice unit, see below for a more precise definition) are highly affected by the monomer distribution, we show that it is possible to fine-tune the polymer's behavior by choosing its knot type. Indeed, topology has strong effects on the behavior of knotted polymer rings, in particular when they are short [51,52]. A considerable effort has been spent here in order to understand the entropic and topological origins of the observed phenomena. In particular, the characterization of the different phases of knotted copolymers, sometimes appearing in a short interval of temperature, has required the introduction of precision experiments of numerical calorimetry. In this way, it has been possible to arrive at a satisfactory understanding of the phase transitions responsible for the various peaks observed in the plots of the specific heat capacity.

Concluding this Introduction, the present analysis requires the sampling of rare conformations in the low energy range that are dominant in the lowest temperature range. For instance, in the case of knotted diblock copolymers having an excess of monomers of one type, the inclusion in the simulations of the lowest energy states is crucial to capture the structural rearrangements that these knots undergo at low temperature. Unfortunately, such conformations are rare and act as bottlenecks in a Markov-chain Monte Carlo simulation [53]. To address this problem, we adopt the Wang-Landau Monte Carlo algorithm [24], whose ability in sampling rare events is well established in the literature, see, e.g., Refs. [54,55]. Following Ref. [56], in this work we have used parallelization techniques to speed up the Wang-Landau algorithm in such a way that it has been possible to include the lowest energy conformations. Some of these techniques have been discussed in more detail in Ref. [57] and Ref. [58].

The material presented in this paper is organized as follows. In Sec. II the used methodology is briefly explained. The thermal properties of knotted copolymer rings in an ion solution are presented in Sec. III. Finally, the conclusions and open problems are the subject of Sec. IV.

II. METHODOLOGY

Polymer rings are modeled as self-avoiding loops on a simple cubic lattice. The rings are knotted and their topology is kept fixed during the simulation. Two consecutive monomers on the loop are linked by one lattice bond, so that the total length of the knot in lattice units is equal to the number of monomers N. We consider monomers of two types: Monomers of type A have a positive charge, while monomers of type B are negatively charged. The monomers are subjected to very short-range interactions that can be attractive or repulsive. In particular, monomers of the same kind

repel themselves, while the interactions between the A and B monomers are attractive.

Our setup is intended to model block copolymers formed by monomers of positive and negative charges fluctuating in a highly screening ion solution. We notice that this setup is relevant not only for ion solutions but also in the case of charged polymers in water. In fact, water is able to screen efficiently the Coulomb interactions. For instance, in water at room temperature the Bjerrum length l_B amounts to just 7 Å. Let us recall that the constant l_B measures the length scale at which the strength of the Coulomb interactions in a dielectric medium becomes equal to the thermal energy $k_B T$, where k_B is the Boltzmann constant and T is the temperature [59].

The energy of a given knot conformation X is expressed by the following Hamiltonian:

$$H(X) = \varepsilon(m_{AA} + m_{BB} - m_{AB}). \quad (1)$$

In Eq. (1) the quantities $m_{MM'}$'s count the numbers of contacts between monomers of the kind M and M', where $M, M' = $ A, B. Two monomers i and j are said to be in contact if $i \neq j \pm 1$ and $|\mathbf{R}_i - \mathbf{R}_j| = 1$. Here $\mathbf{R}_1, \ldots, \mathbf{R}_N$ denote the locations of the N monomers. $\varepsilon > 0$ is an energy scale measuring the cost of one contact, which can be positive or negative. Other setups are possible, see, for instance, Ref. [30] and Refs. [60,61].
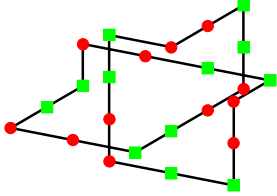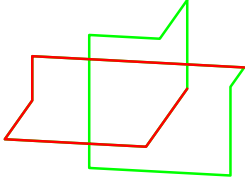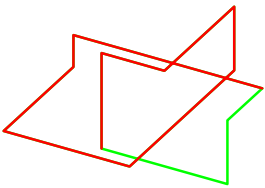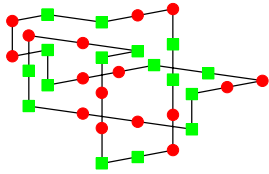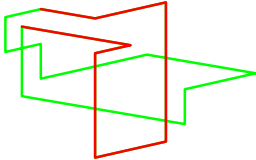
We construct knots containing alternating units with n_A monomers of type A and n_B monomers of type B until the total number of monomers N is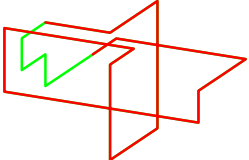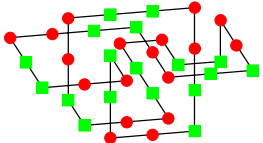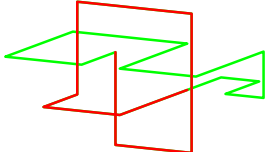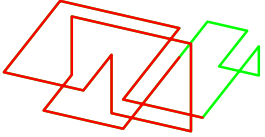 obtained. Knotted multiblock copolymers of this kind will be denoted with the symbol $M(N, n_A, n_B)$. If N is not a multiple of $n_A + n_B$, then a slight excess of monomers of type A is allowed. In the following, it will be convenient to introduce the total number N_A of A monomers and the total number N_B of B monomers. Of course $N_A + N_B = N$. A particularly interesting subcase is that in which the knotted ring is formed starting from a AB diblock copolymer composed by two segments, one with A monomers and the other with B monomers and then circularizing it. Such knotted AB diblock copolymer rings will be distinguished introducing the new symbol $D(N_A, N_B)$. Clearly, $D(N_A, N_B) = M(N, N_A, N_B)$. To further characterize the analyzed systems, also their monomer composition $f = N_A/(N_A + N_B)$ will be used. A summary of the main knot types and monomer compositions investigated in this work is provided in Table I. Uncharged homopolymer knots have already been studied in the past, see for instance Ref. [62], and will thus be important for comparison. In this case, as there are no charges, short-range interactions are used to model the quality of the solvent and the Hamiltonian of Eq. (1) simplifies to

$$H_{hom}(X) = \pm \varepsilon m_{AA}, \quad (2)$$

in which it has been assumed that all monomers are of type A. Homopolymers in a good solvent, corresponding to the $+$ sign in the right-hand side of Eq. (2), will be denoted with the symbol $H_+(N)$ while homopolymers in a bad solvent, corresponding to the $-$ sign, will be denoted with the symbol $H_-(N)$.

Examples of polymers that may be described within the present setup are poly(acrylic acid) block copolymers and DNA. The interaction of DNA with ions has been extensively

TABLE I. Main knot types and monomer compositions f used.

$M(N, n_A, n_B)$	$f = 0.5$	$f = 0.83$
3_1, M(24,2,2)	3_1, D(12,12)	3_1, D(20,4)
4_1, M(32,2,2)	4_1, D(16,16)	4_1, D(27,5)
5_1, M(36,2,2)	5_1, D(18,18)	5_1, D(30,6)

studied, see for instance Ref. [63]. Other examples are reported in Ref. [64], in particular polyelectrolytes based on a poly(p-phenylene) backbone. Similar setups have been used in the case of proteins, see the already-mentioned HP protein model [46].

For convenience, we will introduce the rescaled temperature $T^* = \frac{k_B T}{\varepsilon}$. To go back from T^* to the usual temperature T measured in Kelvins some assumptions on ε are needed. We assume that the strength ε of the interactions is a multiple of the energy associated with thermal fluctuations at room temperature T_0, i.e., $\varepsilon = q k_B T_0$, where $T_0 \sim 298$ K and q is a positive real constant. Choosing different values of the parameter q allows to model different ion solutions. For example, if the ions are multivalent, like Ca^{++} or Mg^{++}, then we expect higher values of q with respect to monovalent ions like Na^+ or Cl^-. Changes in q imply among others changes in the temperatures at which phase transitions occur.

At this point it is easy to see that the temperature T is expressed in terms of T^* as follows: $q T^* T_0 = T$. For example, if $q \sim 1.5$, then the point $T^* = 1$ corresponds to the temperature $T = 1.5 T_0 \sim 447$ K. After the passage $T \longrightarrow T^*$, it

is possible to eliminate the ε factor in the Hamiltonian of Eq. (1). The upshot is that we obtain the following rescaled Hamiltonian: $H^*(X) = \frac{H(X)}{\varepsilon}$. The symbol E will denote the values of $H^*(X)$.

The simulations are performed using the Wang-Landau Monte Carlo algorithm [24]. The initial knot conformations (seeds) are obtained by elongating the existing conformations of minimal length knots [65,66] until the desired final length is attained. Each seed is equilibrated by performing on it random transformations until the criterion for equilibrium of Ref. [67] is fulfilled. Knots up to six crossing according to the Rolfsen table are studied, though there is no restriction against including more complicated knots.

The details on the sampling can be found in Refs. [68] and [62]. The random transformations that are necessary for sampling the different knot conformations are the pivot moves of Ref. [69]. In order to preserve the topological state of the system, the pivot algorithm and excluded area method of Ref. [68] is applied. First, during the sampling a randomly chosen segment s of the knotted copolymer is modified using a pivot move like a reflection, an interchange or an inversion.

Due the fact that the initial and final monomers of s are kept fixed, the new segment s' obtained after the transformation and the old segment s form a closed loop $\ell = s' + s$. If s consists of k segments, then ℓ is composed by $2k$ segments. Next, we check if some part of the knot passes through the internal points of an arbitrary surface spanned by the loop ℓ. If yes, then the pivot move breaks the topology of the knot and is thus rejected. In the opposite case it is accepted. Up to $k = 5$, the surfaces spanning the loop ℓ have been classified in Ref. [68]. There are at most eight of them. This implies that for a knot of N segments the maximum time necessary in order to detect potential topology breakings scales as $8N$.

The partition function of the polymer knot is given by

$$Z(T^*) = \sum_{E=E_{\min}}^{E_{\max}} e^{-E/T^*} g(E), \tag{3}$$

where $g(E)$ denotes the density of states,

$$g(E) = \sum_X \delta(H^*(X) - E). \tag{4}$$

$g(E)$ is the quantity to be evaluated via the Wang-Landau Monte Carlo algorithm. $E_{\min}$ and $E_{\max}$ represent, respectively, the minimum and maximum values of the energy. The whole energy range $\mathcal{I} = [E_{\min}, E_{\max}]$ over which the sampling is performed depends on the used setup, the length of the knot, its topology, and the selected monomer distribution. To determine the values of $E_{\min}$ and $E_{\max}$, a preliminary run without specifying any energy limit is performed. In doing that we exploit the fact that the Wang-Landau algorithm is very efficient in exploring the whole energy range of the system. The preliminary run is stopped when no new values of the energy are found for a reasonably long time. After that, the averages of the observables are computed by a second run with the values of $E_{\min}$ and $E_{\max}$ calculated from the preliminary run. Also in this second run the energy range is kept open, but for the convergence of the Wang-Landau algorithm only the energy values in the interval $[E_{\min}, E_{\max}]$ are considered. For the convergence of the Wang-Landau algorithm the sampling of an order of 10^{12} conformations is necessary. If new values of $E_{\min}$ and $E_{\max}$ appear during the sampling, then the run is repeated with the new, extended energy range. In the case of long polymers with $N \geqslant 300$, cuts in the energy range are necessary in order to obtain the convergence of the Wang-Landau algorithm in a reasonable time. In this case, several runs are repeated by slightly changing the energy range to check that the results are independent of the energy range despite these small variations. It turn out that the Wang-Landau algorithm is very robust in this sense. For instance, small variations of the energy range do not have relevant influences on the height and the position of the peaks of the specific heat capacity. The averages of the observables are particularly insensitive under changes of $E_{\max}$, while variations of a few percentages occur at very low temperatures, i.e., $0 < T^* \leqslant 0.5$, by changing $E_{\min}$.

The expectation values of any observable $\mathcal{O}$ may be computed using the following formula:

$$\langle \mathcal{O} \rangle(T^*) = \frac{1}{Z(T^*)} \sum_{E=E_{\min}}^{E_{\max}} e^{-E/T^*} g(E) \mathcal{O}_E. \tag{5}$$

Here $\mathcal{O}_E$ denotes the average of $\mathcal{O}$ over all sampled states with rescaled energy E. The observables that will be considered in this work are the mean specific energy,

$$\frac{\langle E(T^*) \rangle}{N} = \sum_{E=E_{\min}}^{E_{\max}} \frac{E}{N} e^{-E/T^*} g(E), \tag{6}$$

the specific heat capacity, $C/N = \frac{1}{N} \frac{\partial \langle E(T^*) \rangle}{\partial T^*}$, and the mean-square average of the gyration radius, R_G^2. An important role is played by the averages of the numbers of contacts m_{AA}, m_{BB}, and m_{AB} formed by the monomers of a specific type with themselves or with the other type. Also the averaged total number of contacts, $n_{\mathrm{tot}} = m_{\mathrm{AA}} + m_{\mathrm{BB}} + m_{\mathrm{AB}}$, will be relevant in the following. These variables are necessary to understand the behavior of knotted copolymer rings in the presence of monomers of different type, in which there are not only compact or swollen states but also mixed or unmixed states. The average values of $m_{\mathrm{AA}}, m_{\mathrm{BB}}, m_{\mathrm{AB}}$, and n_{tot} are plotted in Fig. 1 for a knot 4_1 in two monomer distributions that will be relevant for the future discussion.

Let us recall that in the Wang-Landau algorithm the sampling is performed in the microcanonical ensemble, in which the energy, not the temperature, is a thermodynamic variable. This makes it difficult to inspect the conformations near the transition points. For this reason, during our simulations snapshots of conformations at different energies are stored covering as much as possible the interval $[E_{\min}, E_{\max}]$. Once the simulation finishes, Eqs. (5) and (6) are used to plot the specific heat capacity and the average energy $\langle E \rangle$ against the temperature. The temperature at which a given phase transition is occurring is determined by looking at the peaks of the specific heat capacity. The average values of the energy of the conformations near the transition point are known from the plot of $\langle E \rangle$. At this point, the previously stored conformations whose energies are slightly below or above the energy at the transition point are inspected. Such conformations provide invaluable information that may be used to understand the rearrangements undergone by knotted polymer rings during the transition. As previously mentioned, the transitions taking place at low temperatures involve very rare states whose conformations are difficult to be captured. For example, states with energy $E_{\min} = -60$ in a 3_1 knot with $N = 90$ and monomer distribution $D(70, 20)$ have a probability $P(E) = \frac{g(E)}{\sum_E g(E)}$ of being generated by random transformations that is below 10^{-30}. This complicates the sampling process, especially when knots are long. In a knot 4_1 with $N = 1000$ and monomer distribution $D(800, 200)$, the lowest energy state has a probability lower than 10^{-256}.

III. RESULTS: THERMAL PROPERTIES OF KNOTTED BLOCK COPOLYMER RINGS

We report the effect of monomers distribution and topology on copolymers of different lengths. We focus in particular on multiblock copolymers with repeating blocks of monomers of type A and B and diblock copolymers with either the same number of monomers of type A and B, or an excess of monomers of one type. Interestingly, the first setup has been considered in Ref. [70], where the dynamics of the unknotting
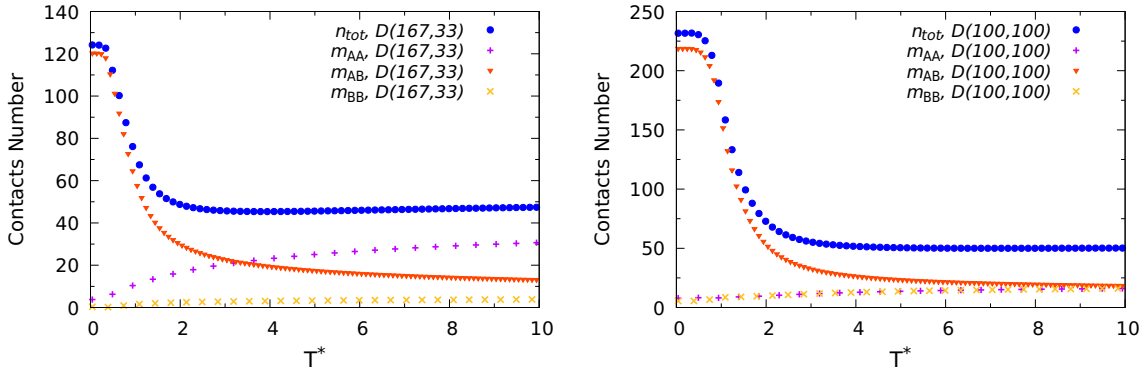
FIG. 1. This figure shows how the numbers n_{tot}, m_{AA}, m_{AB}, and m_{BB} change with the temperature in the case of a knot 4_1 with monomer distributions $D(167, 33)$ (left panel) and $D(100, 100)$ (right panel).

has been investigated. The second setup is similar to that investigated in Ref. [40]. The topologies here include the knots 3_1, 4_1, and 5_1, as well as knots 6_1 and 10_{122} as test cases.

The variety of behaviors that it is possible to obtain in the case of short copolymer knots is shown in Fig. 2 which reports the diagrams of the gyration radius and the heat capacity of a trefoil knot 3_1 of length $N = 90$ in different monomer distributions. For convenience, in the following we will use the word knot to mean knotted polymer ring.

A. Effects of the choice of monomer distribution on short polymers

As shown in Fig. 2 (left panel), the distribution of the A and B monomers greatly influences the range of allowed gyration radii. For example, in the 3_1 copolymer knot with monomer distribution $D(80, 10)$, the values of the mean-square gyration radius are restricted to the narrow interval $13 \leqslant R_G^2 \leqslant 16$. By passing to the $D(75, 15)$ distribution, a change that requires just the substitution of five monomers of type A with monomers of type B, the new range in which R_G^2 can take its values is $7.86 \leqslant R_G^2 \leqslant 14.89$. Let us note that all gyration radii in Fig. 2 (left panel) converge to a common limit at the highest temperatures considered here (data not shown) as is expected when the interactions between the monomers are no longer relevant due to the strong thermal fluctuations.

Approximately, at $T^* \to +\infty$ the value of the mean-square gyration radius R_G^2 lies in the range 13.21–13.86. A better estimation is difficult because of the statistical errors.

Also the heights of the peaks of the specific heat capacity and the temperatures at which these peaks occur are very sensitive to the monomer distribution as it is possible to realize from Fig. 2 (right panel). The peaks' heights range in fact from about 0.11 for knotted and uncharged homopolymers in a good solvent [monomer distribution $H_+(90)$], see the plot at the bottom of Fig. 2 (right panel) and comments in the caption) up to about 4.00 in the case of the multiblock copolymer $M(90, 2, 2)$ (Fig. 3, left panel). In the case of diblock copolymer rings, we observe a profound difference between the behavior of knots with monomer distribution $D(45, 45)$ and knots with monomer distribution $D(75, 15)$. This point will be discussed later in more detail. Finally, we note that the temperature at which the peak of the specific heat capacity appears can be fine-tuned by choosing the monomer distribution.

B. Effects of topology in short polymers

The effects of topology for short polymer knots are illustrated in Fig. 4, where the plots of the gyration radii and of the specific heat capacity for a few AB diblock copolymers of knot types 3_1, 4_1, and 5_1 are presented. For each knot
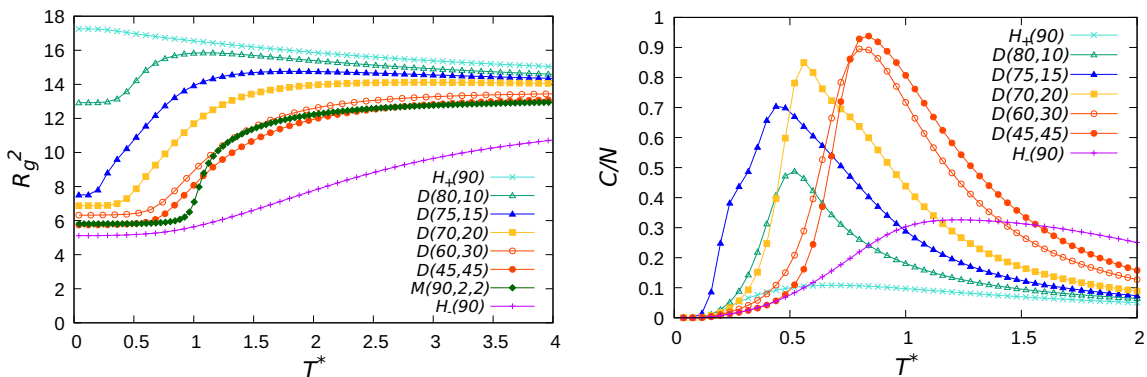

FIG. 2. The mean-square gyration radii R_G^2 (left panel) and the specific heat capacities C/N (right panel) of a knot 3_1 with $N = 90$ in various monomer distributions are plotted as functions of T^*. In the left panel, going from the top to the bottom, it is possible to distinguish the plots of the gyration radii for the following monomer distributions: $H_+(90)$, $D(80, 10)$, $D(75, 15)$, $D(70, 20)$, $D(60, 30)$, and $D(45, 45)$. The plot in the bottom part of the left panel is that of the homopolymer in a bad solvent $H_-(90)$.
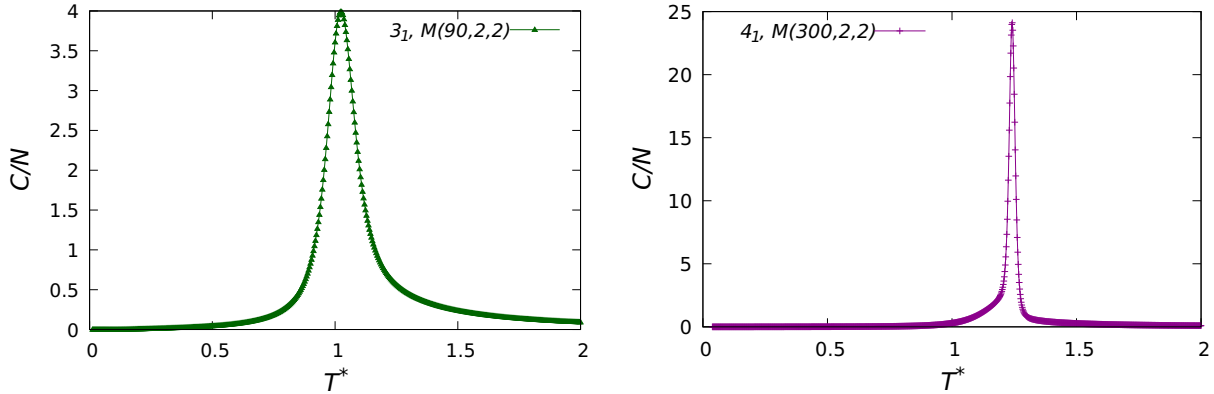
FIG. 3. Plots of the specific heat capacity of knotted multiblock copolymers with monomer distribution $M(N, 2, 2)$ for the lengths $N = 90$ (left panel) and $N = 300$ (right panel). We notice that the specific heat capacity of these knots exhibits just a single peak that is higher than those of the knots with other monomer distributions, see for example Fig. 4 for short polymers and Fig. 5 for long polymers. Moreover, the single peak appears at $T^* > 1$, contrarily to what happens in all other monomer distributions in which $T^* \leqslant 1$ when $N \leqslant 300$.

type, two different monomer distributions have been taken into account, namely $D(45, 45)$ and $D(75, 15)$. Fixing the monomer distribution and the knot length, which is equal to $N = 90$, we expect that the differences in the plots are solely due to pure topological effects. The latter are quite evident in the figure if we look only at the plots of the gyration radii of the knots with the same monomer distribution, i.e., $D(45, 45)$ or $D(75, 15)$. It turns out from Fig. 4 that the choice of the knot type significantly affects the gyration radius and the heights of the peaks of the specific heat capacity. There is also a visible shift of the temperature in which the transition from the compact to the expanded state occurs.

C. Effects of the monomer distribution and topology on longer polymers

Figure 5 illustrates how topology and monomer distribution affect the gyration radius (left panel) and the shape of the peaks of the specific heat capacity (right panel) of longer knots with $N = 200$ [71].

As in shorter polymers, the behavior of knotted diblock copolymers with $N \geqslant 200$ strongly depends on the monomer composition f, see Fig. 5 in which the monomer distribution $D(100, 100)$ corresponds to $f = \frac{1}{2}$ and the monomer distribu-

tion $D(167, 33)$ corresponds to $f \sim 0.83$. For this reason, in the following we will divide the knotted AB diblock copolymers in the two classes $N_A \gg N_B$ and $N_A \sim N_B$. The specific heat capacity of knots with $N_A \gg N_B$ exhibits a double peak or a peak with a shoulder in the case of 5_1, while that of knots with $N_A \sim N_B$ has only one peak. For knotted polymers with $N = 200$, the threshold value of the monomer composition f that separates the two classes has been identified to be between $f \sim 0.785$ and $f \sim 0.800$. These values correspond to $N_A = 157$, $N_B = 43$ and $N_A = 160$, $N_B = 40$, respectively (data not shown). In knotted polymers with $f < 0.785$ the specific heat capacity has no double peak and a double peak (or a peak with a shoulder) certainly appears when $f \geqslant 0.800$. It is particularly difficult to determine more precisely the exact threshold value of f because the simulations in the critical range $0.785 \leqslant f \leqslant 0.800$, where the passage from single to double peak is occurring, require a time-consuming exploration of the energy landscape in order to find those low-temperature conformations that are relevant for the structural rearrangement leading to the double peak.

Another characteristic that distinguishes knotted polymers of any length with $N_A \sim N_B$ from those with $N_A \gg N_B$ is that the highest peak of the specific heat capacity is decidedly higher when $N_A \sim N_B$, see Fig. 5 (right panel). This means
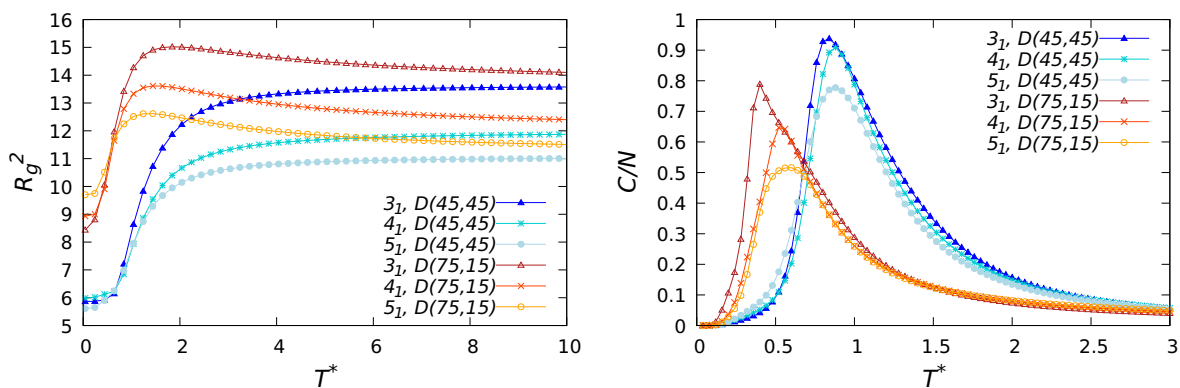

FIG. 4. Presented are the plots of R_G^2 and C/N in the case of the knots 3_1, 4_1, and 5_1 with $N = 90$. This picture shows the differences in the behavior of knotted polymers due to topology when the monomer distribution is fixed. The two cases of monomer distributions $D(45, 45)$ and $D(75, 15)$ are displayed.
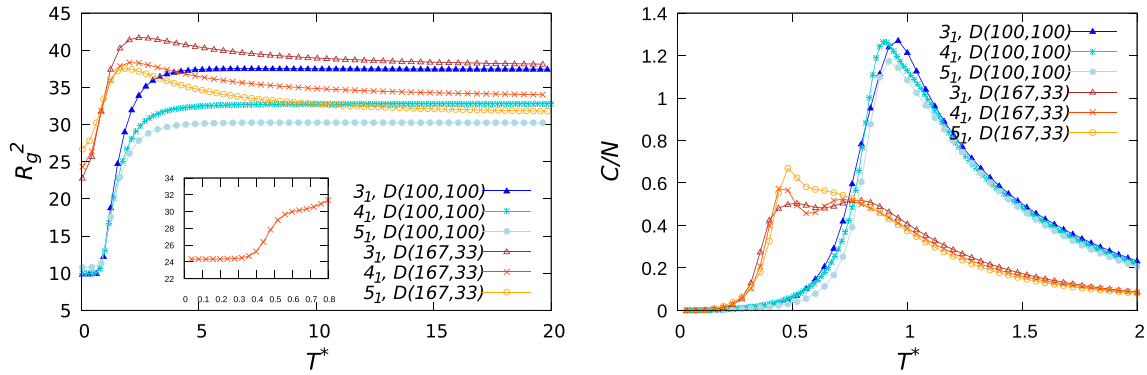
FIG. 5. Dependence of the mean-square gyration radius R_G^2 and of the specific heat capacity C/N on the topology and on the monomer composition f in the case of AB diblock copolymers. Presented are the plots of R_G^2 in the case of the knots 3_1, 4_1, and 5_1 with $N = 200$. For each knot two values of f are considered: $f = 0.50$, corresponding to the monomer distribution $D(100, 100)$, and $f \sim 0.83$, corresponding to the monomer distribution $D(167, 33)$. In the inset of the left panel it is shown a detail of the behavior of R_G^2 for the knot 4_1 with monomer distribution $D(167, 33)$.

that the energy differences between the compact states at low temperatures and the expanded states at high temperatures are not so strong when $N_A \gg N_B$. This is due to the fact that the number of contacts between the A and B that can be formed in order to minimize the energy according to the Hamiltonian (1) is limited if $N_A \gg N_B$. In general, when the number of A monomers is increased while keeping N fixed, the peaks of the specific heat capacity become lower and lower.

To conclude this discussion, we remark that the behavior of the knot does not change if the monomers of type A and B are interchanged, i.e., $N_A \longleftrightarrow N_B$. For this reason, the situations in which $N_A \gg N_B$ and $N_B \gg N_A$ are equivalent.

Figure 5 further shows that topology has important effects also in the case of longer polymers with $N = 200$. In particular, when $T^* \to \infty$, the asymptotic values of R_G^2 for knots 4_1 and 5_1 are very similar to each other, but this is not the case of knot 3_1. In general, however, we observe that, as in the homopolymeric case [62], topological effects become less marked with growing polymer lengths. A possible explanation of this fact is the following. We notice that the path of a fluctuating polymer is characterized by many turns that are forming for entropic reasons. In the presence of turns, monomers get closer to each other, so that their interactions become more frequent. In a knot, part of these turns is dictated by the topological constraints. As an upshot, one of the effects of increasing the topological complexity by keeping the length fixed is to increase the frequency of the interactions with the consequent changes in the behavior of the knot. The shorter the knot, the larger grows the fraction of turns related to topology with respect to those related to entropy. Thus, it can be expected that in shorter knots topology will have a greater influence than in longer knots, where the majority of turns is of entropic origin. For example, on a simple cubic lattice the minimal trefoil knot has a length $N_{min} = 24$. Supposing that the turns are uniformly distributed along the length of the path, it is possible to estimate that at least one third of the total number of turns is necessary to characterize the topology of a trefoil knot with $N = 72$ monomers. As a consequence, the contribution of topology to the behavior of such a short knot will be much greater than in the case of a trefoil knot

with $N = 240$ in which the knotted part can be confined in just 1/10th of the total length available.

D. Phases of knotted copolymer rings

1. Lamellar phase

A particularly interesting case is provided by knotted polymers with monomer distributions $M(N, 2, 2)$. In contrast to all other cases studied here, they form compact states that are stable also at temperatures $T^* > 1$ and the transition to the expanded phase is much sharper. Consequently, their specific heat capacities are characterized by a single peak which is much higher and narrower than that of all other monomer distributions as it can be realized by comparing the plot of C/N in Fig. 3 (left panel) with the plots in Fig. 2 (right panel). This sharp peak corresponds to the transition from a lamellar phase, characterized by layers of A monomers followed by layers of B monomers, to an expanded phase, which is disordered and with a low mixing between the A and B monomers. The peculiar way in which the monomers of type A and of type B are organized in the lamellar phase in order to minimize the energy at low temperatures is shown in Fig. 6 for a 4_1 knot. Simulations performed considering knotted copolymers with knot type 4_1 and different lengths $N = 90, 200, 480, 720$ show that, by increasing the size of the repeating unit in the multiblock copolymer, for instance choosing $M(N, 3, 3)$, $M(N, 4, 4)$, $M(N, 5, 5)$, etc., the lamellar phase disappears, while the single peak of the heat capacity becomes rapidly lower and wider.

The lamellar phase is not related to a particular topology as it has been observed in all investigated knot types including the unknot 0_1 and the knot 10_{122}. These results have been obtained on simple cubic lattices which are somewhat special, as they are bipartite, meaning that they could be divided into two sublattices S_1 and S_2 such that particles belonging to a sublattice can interact only with particles of the other sublattice. Naively, the absolute minimum of the energy on a bipartite lattice would correspond to all A monomers located on the vertices of S_1 and all B monomers on the vertices of S_2. However, such a structure is not compatible with the connectivity of knotted copolymers with monomer distribution $M(N, 2, 2)$.
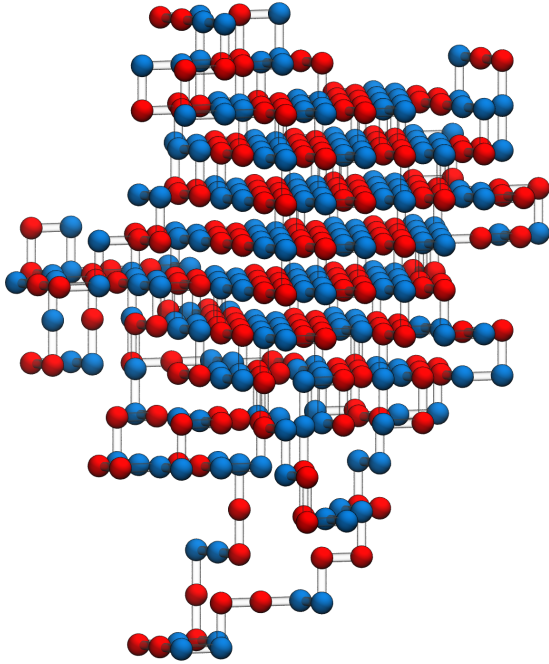
FIG. 6. This picture shows the organization at the lowest temperatures of a knot 4_1 of size $N = 480$ and monomer distribution $M(480, 2, 2)$. As it is possible to see, the monomers are forming layers of A monomers followed by B monomers.

The structure of the found lamellar phase is visible in Fig. 6 and is summarized in Fig. 7. Contiguous monomers form on each plane in the lattice long straight lines along a chosen direction, let us say the x direction. If a monomer of A type is at the point x_i, y_j, z_k, where i, j, k can be any integer number, then its neighbors in the y and z directions are of the B type. It is easy to see that in this way lamellae are formed inside the bulk of the knot along the directions pointed out by the green lines in Fig. 7. Of course, a real knotted copolymer is not bound to a particular lattice and its underlying symmetry group but spontaneously chooses conformations with the suitable symmetry to minimize its energy. The question is if the absolute minimum is attained within a simple cubic lattice or if there is some other lattice which allows the system to reach lower energies. To decide which is the minimum energy of the system extensive calculations using different lattices or off-lattice are required, which would be outside the purpose of this work. Such calculations have been performed for instance in Ref. [72] in which the somewhat related case of spherelike micellar phases in a melt of diblock copolymers is discussed.
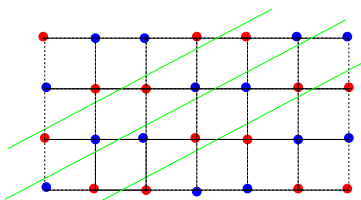

FIG. 7. Sketch of the the organization of knotted polymers in the lamellar phase. Only a cross section along the xy plane is shown. Monomers laying on horizontal lines are connected together. The green lines show the orientation of the lamellae.

It turns out from that work that the minimal energies per chain obtained in all considered lattices vary within a 1% range.

2. Phases of AB diblock copolymers with $N_A \sim N_B$

In knotted AB diblock copolymer rings both attractive and repulsive interactions are simultaneously at work. Despite the repulsive component, when $N_A \sim N_B$ the behavior of these copolymers is similar to that of homopolymers in a bad solvent in which the interactions are purely attractive. The reason is that if the number of A and B monomers is comparable, then a relatively large number m_{AB} of contacts can be formed. This leads to compact conformations held together by the bonds between the A and B monomers at very low temperatures ($0 < T^* \leqslant 0.5$), when m_{AB} is maximized in order to minimize the energy. Of course, due to the repulsions between the monomers with the same charge, the lowest energy conformations cannot be so compact as those formed by homopolymers in a bad solvent, where all interactions are attractive. Nevertheless, when copolymers with $N_A \sim N_B$ are heated, their mean-square gyration radius exhibits a considerable increase of up to 350% in the case of the knot 3_1 with monomer distribution $D(100, 100)$. Similarly to what happens in knotted homopolymers in a bad solvent, the low energy states are quite stable. The swelling process occurs at relatively high temperatures—the specific heat capacity is peaked at $T^* \sim 1$—and continues also when the temperature exceeds $T^* \sim 1$ by a few degrees. The result is a single broad peak in the specific heat capacity with the maximum of the peak at a temperature of $T^* \sim 1$, see Figs. 4 (right panel) and 5 (right panel).

The fact that at very low temperatures there is a large number of contacts between the A and B monomers implies that the compact conformations are characterized by a high level of A-B mixing. On the contrary, the number m_{AB} drastically decreases at $T > 1$, hinting to a possible unmixed phase which is confirmed by close inspection of the stored conformations. The aspects of knot localization, see e.g. Refs. [73] and [74], will be treated elsewhere.

3. Phases of AB diblock copolymers with $N_A \gg N_B$

At very low temperature, $0 < T^* \leqslant 0.5$, knots with $N_A \gg N_B$ are in a compact state with high A-B mixing. At high temperatures they are found in a swollen state and the mixing of A and B monomers is negligible. This behavior is similar to that observed when $N_A \sim N_B$, but due to the condition $N_A \gg N_B$, the differences of the gyration radius between the compact and expanded states are much less marked. The new feature of knots with $N_A \gg N_B$ is an extra peak or a shoulder appearing in the plots of the specific heat capacity of Fig. 5, right panel. The presence of these extra peaks and/or shoulders is a general characteristics of long knotted polymers in which there is an excess of monomers of one type that was also observed in the unknot 0_1 and the knot 6_1 (not shown in this paper). Of course, when the number of A monomers is increased more and more, the double peaks merge into a single one. Eventually, in the limit $f \rightarrow 1$, the case of homopolymers in a good solvent already described in Ref. [68] is recovered.

It is known that double peaks and peaks with shoulders in the plots of the specific heat capacity of polymer chains are
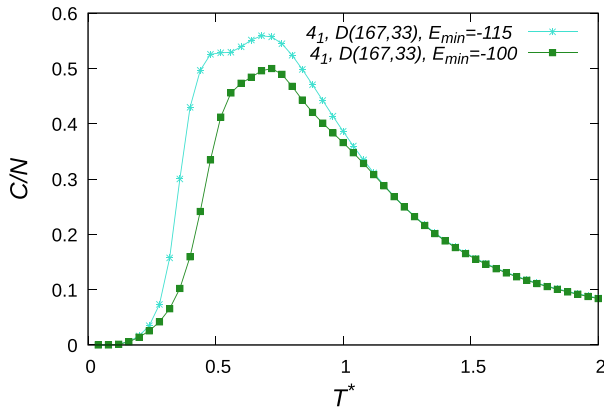
FIG. 8. Plots of the specific heat capacity of a knotted polymer 4_1 with $N = 200$ and monomer distribution $D(167, 33)$ obtained by putting a cutoff $E_{min}^{cutoff} = -100$ (green line) and without a cutoff ($E_{min} = -115$, cyan line). The broad peak in the case with cutoff and the second peak in the case without cutoff almost overlap and appear in the temperature interval in which the polymer undergoes the main expansion process.

related to the occurrence of two different phase transitions in a small interval of temperatures, see Refs. [75–78] and Ref. [36] in the case of polyelectrolytes. The behavior of the specific heat capacity that is observed here is similar to what is found in the transition from the native to the unfolded state in long proteins [79]. That transition is not a simple two-state transition due to the presence of intermediate states. The question is What are the intermediate states in the case of knotted diblock-copolymers with $N_A \gg N_B$?

To answer this question we have performed a series of numerical experiments. First, we have studied the changes occurring in the thermal behavior of several polymer topologies and lengths when the interval of available energies $[E_{min}, E_{max}]$ is gradually decreased from below while keeping constant the upper energy limit E_{max}. Clearly, if there is an intermediate phase transition related to the first peak of the specific heat capacity at low temperatures, then we expect that this peak will disappear when the cutoff E_{min}^{cutoff} in the restricted energy interval $[E_{min}^{cutoff}, E_{max}]$ is such that the low-energy

states responsible for this transition are no longer allowed. Indeed, this is exactly what is observed: The first peak at low temperatures disappears, leaving only one broad peak after a certain threshold value E_{min}^{cutoff} is reached. For instance, for a knot 4_1 with $N = 200$ and monomer distribution $D(167, 33)$, the first peak is absent by choosing $E_{min}^{cutoff} > -105$, see Fig. 8. All that hints to the fact that the first peak is due to a rearrangement of the polymer corresponding to the transition to an intermediate phase.

Further evidence of a rearrangement is a characteristic pattern that is visible in the plots of the mean-square gyration radius R_G^2. An example of such patterns is shown in the inset of Fig. 5 (left panel), in which the plot of R_G^2 of a knot 4_1 with monomer distribution $D(167, 33)$ is displayed in greater detail. We can see that there is a rapid increase of R_G^2 in the range of temperatures $0.4 \leqslant T^* \leqslant 0.6$. This range coincides approximately with that in which the first peak of the specific heat capacity of the knot 4_1 centered at about $T^* = 0.50$ is appearing; see the inset in Fig. 5 (left panel). Another hint suggesting that knotted diblock copolymers with $N_A \gg N_B$ have an intermediate phase comes from the close inspection of the stored knot conformations at different energies. The available data obtained from simulations encompassing several knot topologies and lengths in the range $200 \leqslant N \leqslant 500$ suggest that there are three distinct phases: "unmixed," "mixed," and "intermediate" or U, M, and I phases. At low temperatures the knotted polymer is in the M phase, characterized by relatively compact conformations and by a strong mixing of the A and B monomers. The structure of these conformations is heterogeneous; however, it is possible to distinguish a well-defined compact bulk held together by the bonds formed by the A and B monomers. A number of short tails containing A monomers is departing from this bulk, see Fig. 9 (left panel). The presence of such tails is unavoidable because, due to the excess of the A monomers with respect to the B monomers, not all A monomers may be accommodated in the bulk. When the temperature increases, the knotted polymer undergoes a first transition, entering in the I phase. Also in the I phase a compact bulk is observed, but the tails protruding from it are decidedly longer, see Fig. 9 (right panel). The passage from the M phase to the I phase is at the origin of the first peak in

Knot 4_1, $N=200$, $D(167,33)$, $E=-105$
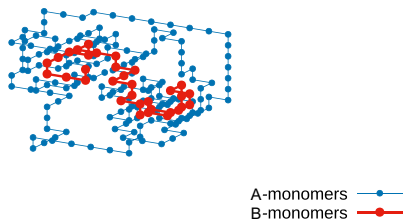
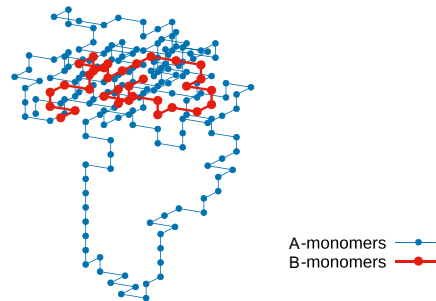Knot 4_1, $N=200$, $D(167,33)$, $E=-100$

FIG. 9. This figure shows two sample conformations of a knot 4_1 with length $N = 200$ and monomer distribution $D(167, 33)$. The conformation in the left panel has energy $E = -105$ and is an example of conformations in the M phase. The conformation in the right panel has energy $E = -100$ and it is a representative of the I phase, see Fig. 10 and related comments. It is characterized by a partially ordered portion located in the upper part of the knot in which some of the A monomers are in contact with the B monomers. Other A monomers form a "tail" that is visible on the bottom of the knot. Both pictures have been drawn using the same dimension scale.
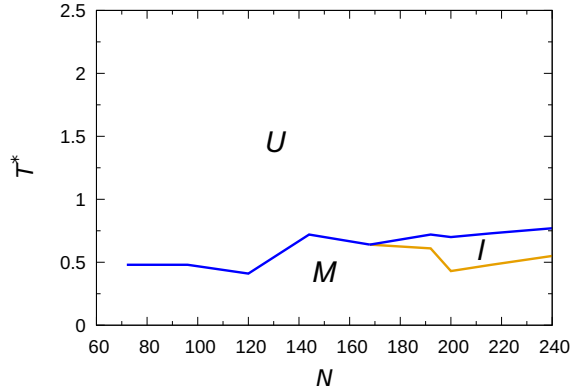
FIG. 10. Phase diagram in the plane (N, T) of knotted AB diblock copolymers with fixed monomer composition $f = \frac{5}{6}$ and knot type 4_1. The diagram has been obtained using the data coming from a set of nine simulations, each of them characterized by a different number of monomers N: $N = 72, 96, 120, 144, 168, 192, 200, 216,$ and 240.
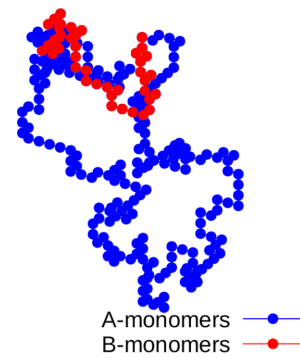

FIG. 11. A typical conformation in the U phase (see Fig. 10). The knot appears in a swollen state and the mixing between the A and B monomers is negligible. The conformation in this plot is that of a knot 4_1 with length $N = 240$, monomer distribution $D(200, 40)$, and energy $E = -20$.

the specific heat capacity at temperatures $T^* \leqslant 0.5$. The main swelling process leading to the unmixed, relatively swollen U phase causes the second, broad peak in the plot of the specific heat capacity. Indeed, comparing the plots of R_G^2 and C/N, see for instance Fig. 5 (left and right panels), it is possible to see that the main expansion of the knotted polymers takes place in the range of temperatures where the second peak is appearing.

The phase diagram of knotted AB diblock copolymers with fixed knot type 4_1 and fixed monomer distribution such that $N_A \gg N_B$ is presented in Fig. 10. This figure has been obtained by first drawing on the (N, T) plane the points corresponding to the peaks of the heat capacity of nine knotted copolymers 4_1 with different number of monomers in the range $72 \leqslant N \leqslant 240$, see the caption of Fig. 10 for more details. Next, these points have been connected with lines. These lines separate the various phases. To be sure that there are no effects due to the change of monomer distribution, it has been required that, independently of N, the monomer composition for all knots is always $f = 5/6$. For instance, for $N = 72$ we have put $N_A = 60$, $N_B = 12$ and for $N = 144$, $N_A = 120$, $N_B = 24$. The plane (N, T) has been chosen because it is the analog in the present case of the (V, T) plane in the standard thermodynamics of gases. We note that the lines in the phase diagram of Fig. 10 have a bifurcation approximately when $N = 192$. After this threshold, the knotted AB diblock polymers 4_1 with $N_A \gg N_B$ exhibit three phases. In Fig. 10 the bifurcation point appears at a lower value, but this is only due to the limited resolution in the N axis. A representative conformation of the U phase is presented in Fig. 11. An analogous phase diagram may be drawn in the case in which the knot type is 3_1 or 5_1. In the latter case, however, the third phase appears when the number of monomer is higher than 200.

A last point to clarify is why there is a set of conformations at low temperatures that are so stable to produce measurable effects and constituting a new, intermediate phase. After all, when a knotted polymer in a compact state typical of very low temperatures is heated, it could be expected that, in the initial phase of the expansion, its compact conformation will

start to get "frayed." This means that the weak thermal fluctuations are only able to melt the external part of the knotted polymer, while the main compact bulk is still held together by the bonds between the A and B monomers. This fraying process produces tails similar to those that characterize the conformations in the I phase and can be observed also in knotted polymers with monomer distribution $N_A \sim N_B$. So what is the mechanism behind the stability of these conformations? To unravel this puzzle, we have performed additional numerical tests with the aim of exploring the energy landscape of knotted AB diblock copolymers. The idea is that if there is an intermediate phase appearing together with the mixed M phase in a short range of temperatures, then the free energy of the system should exhibit two close minima corresponding to the M and I phases as shown in Fig. 12. As a consequence, there should be conformations in the low part of the energy interval near these minima that, despite having the same energy E, have different features because they belong
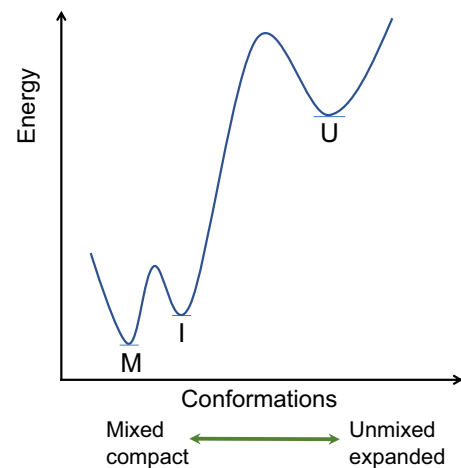

FIG. 12. Pictorial representation of the energy landscape of knotted copolymer rings with $N_A \gg N_B$. The three minima corresponds to the three phases U, I, and M described in the text.
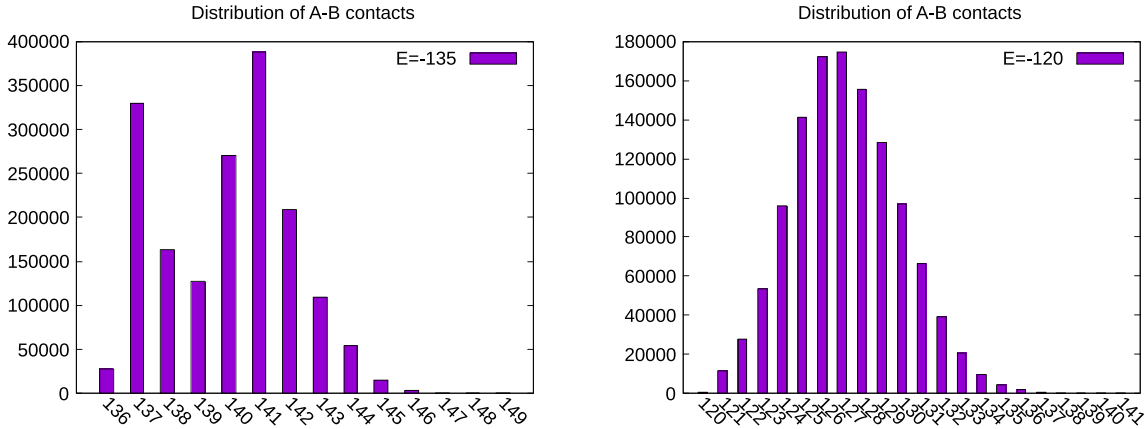
FIG. 13. The histograms $H_E(m_{AB})$ in this picture show the distribution of the number of contacts m_{AB} in conformations of fixed energy E. The data have been obtained by counting the number of contacts m_{AB} in all conformations with energy $E = -135$ (left panel) and energy $E = -120$ (right panel) sampled during a run that computed the density of states of a knotted diblock copolymer 3_1 with $N = 240$ and monomer distribution $D(200, 40)$. The possible values of m_{AB} range in the interval $136 \leqslant m_{AB} \leqslant 149$ when $E = -135$ and $120 \leqslant m_{AB} \leqslant 141$ when $E = -120$. The distribution of m_{AB} has two peaks centered in $m_{AB} = 137$ and $m_{AB} = 141$, respectively, in the case $E = -135$ and is Gaussian with most probable value in $m_{AB} = 127$ in the other case.

to different minima. In order to capture these differences, we have measured the histogram $H_E(m_{AB})$ of the number of contacts formed by the A and B monomers in conformations with a given energy E. Clearly, $H_E(m_{AB}) = 0$ if $m_{AB} < E$. The obtained results confirm the existence of two types of conformations at very low temperatures. As we see from Fig 13 (left panel), the histogram $H_E(m_{AB})$ of a knot 4_1 with $N = 240$ and monomer distribution $D(200, 40)$ exhibits two peaks in the case of conformations of energy $E = -135$, i.e., in the lowest energy domain ($E_{min} = -140$). With increasing energy, the m_{AB} histogram becomes a Gaussian centered at the most probable value of m_{AB}. An example of such histograms when $E = -120$ is shown in Fig. 13 (right panel). Numerical experiments have been performed changing the knot topology, the monomer distribution, and the polymer length. The data show that whenever the plot of the specific heat capacity has a double peak, in the low-energy spectrum the histogram $H_E(m_{AB})$ is characterized by a double peak, too. Moreover, when the energy E is near to the absolute energy minimum E_{min}, the most probable value of m_{AB} is slightly higher than E. In conclusion, in agreement with the hypothesis of the existence of an intermediate phase, knotted polymers with monomer distributions such that $N_A \gg N_B$ have two kinds of low-energy conformations characterized by two different values of the number of A-B bonds. The states in the M phase are assigned to the first peak in the m_{AB} histogram, in which the value of m_{AB} is closer to that of the energy E of the state. The intermediate states in the I phase are assigned to the second peak of $H_E(m_{AB})$, in which the number of A-B bonds is somewhat higher. This small excess of A-B bonds is sufficient to stabilize these states against the weak thermal fluctuations in the interval of low temperatures in which the I phase is observed. This stabilizing mechanism is not supported in knotted polymers with $N_A \sim N_B$ because they form stronger compact states that start to melt at high temperatures, where the thermal fluctuations are too strong.

In shorter knots, with $N = 90$, only a single peak is observed. One possible explanation is that in a short knot the

interactions between the monomers are more frequent than in a long one. In this situation, a rearrangement that increases the number of contacts between the A and B monomers will also bring closer monomers of the same type that are subjected to repulsive interactions. It is thus very likely that such rearrangement will be penalized from the energetic point of view.

Finally, since the A monomers are numerous in the case $N_A \gg N_B$ and are subjected to repulsive interactions, we may expect that, at high temperatures, the knot will shrink as homopolymers in a good solvent do. The plots of the gyration radius show indeed that also knotted diblock copolymers are subjected to this shrinking process but to a lesser extent than homopolymers, see for instance Fig. 5 (left panel). While the shrinking produces in homopolymers just a small peak in the specific heat capacity, in the present case its effects on the plots of C/N are negligible.

E. The case of knots with $N \geqslant 300$

The data of longer knots with $N = 300$ and $N = 500$ agree with the previous conclusions, see Figs. 14 and 15. We note that three peaks appear in the plot of the specific heat capacity of the knot 4_1 with $N = 300$ and monomer distribution $D(250, 50)$; see Fig. 14 (right panel). This is compatible with the fact that more than one rearrangement could occur in longer polymers when $T^* < 1$. In agreement with the characteristic pattern of these rearrangements mentioned in Sec. III D 3, the inset in the left panel of Fig. 14 shows a rapid growth of the gyration radius in correspondence of the first peak at about $T^* \sim 0.35$. However, at the temperature $T^* \sim 0.55$ of the middle peak the plot of R_G^2 becomes almost flat. The explanation of this flat region and the identification of the processes causing these peaks would require a more extended analysis like that performed in the case of knots with $N = 200$.

Finally, the data of the specific heat capacity displayed in Fig. 15 confirm that also long knots with $N = 500$ have
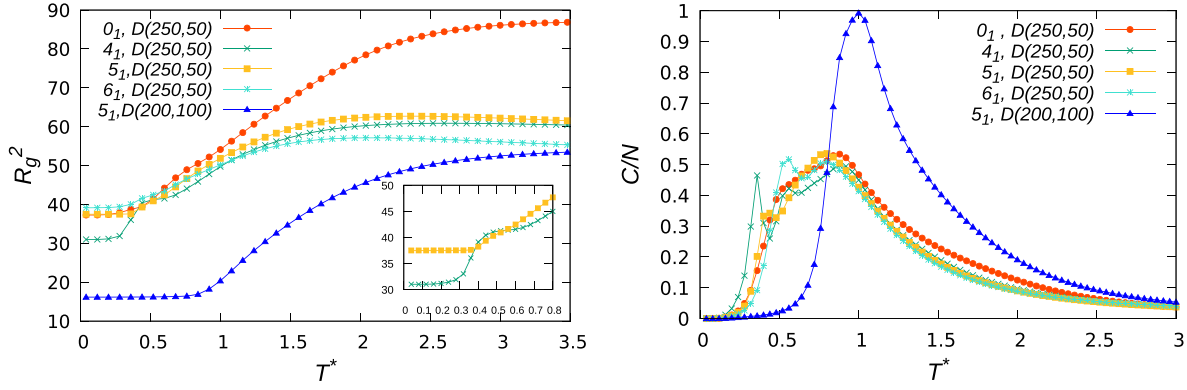
FIG. 14. The data of the gyration radius R_G^2 of knots 0_1, 4_1, 5_1, and 6_2 of length $N = 300$ and monomer distribution $D(250, 50)$ are presented. In the case of knot 5_1 it is shown the plot of R_G^2 also for the monomer distribution $D(200, 100)$. In the inset the behavior of the gyration radius of knots 0_1 and 4_1 is displayed in more details at low temperatures. Note the characteristic saddle point in the plot of the gyration radius of knot 4_1 at $T^* \sim 0.45$.

a different behavior depending if $N_A \sim N_B$ or $N_A \gg N_B$. In particular, no double peak is observed in the case $N_A \sim N_B$.

IV. CONCLUSIONS

In this work the Wang-Landau algorithm has been applied to study the thermal properties of a lattice model of charged knotted copolymer rings in a ion solution with the monomers subjected to very short-range interactions. A- and B-type monomers carry opposite charges.

While uncharged homopolymers are simple systems whose mean-square gyration radius steadily increases (in bad solvents) or slightly decreases (in good solvents) with growing temperatures, knotted copolymers exhibit a more complex behavior with several new features that may be tuned by changing their monomer distribution and topology. Knotted multiblock copolymers with monomer distribution $M(N, 2, 2)$ turn out to be special: Their specific heat capacity is characterized by a single, very high peak concentrated in a narrow range of temperatures, as reported in Fig. 3 (left and right panels). The data of the gyration radius show that, exactly in this range of temperatures, such knots undergo a sharp swelling process similar to that of the homopolymer chains studied in Ref. [34]. A close inspection of the knot conformations has

shown that these knots are in a lamellar phase at very low temperatures, see Fig. 6. In all other monomer distributions of the kind $M(N, n_A, n_B)$ that have been investigated here, the knot expansion is much smoother and occurs at decidedly lower temperatures.

Knotted diblock copolymers with monomer distributions $D(N_A, N_B)$ can be divided into two classes depending if $N_A \sim N_B$ or $N_A \gg N_B$. Knots with monomer distributions belonging to the first class behave similarly to chargeless homopolymers in a bad solvent. In particular, they are found in a compact state at very low temperatures and expand with rising temperatures. This expansion is responsible for a single high and broad peak in their heat capacities that is centered at relatively high temperatures, with $T^* > 1$ in the case of longer polymers with $N \geqslant 300$. When $N_A \gg N_B$, instead, the expansion has a more limited range and, in comparison with knots with $N_A \sim N_B$ of the same length, it occurs at lower temperatures. States in both classes are better characterized by the level of mixing between the A and B monomers than by the mean-square gyration radius. The role of the phase separation was stressed also in the case of copolymer chains in Ref. [80]. It is possible to distinguish a mixed, relatively compact M phase at the lowest temperatures and an unmixed, relatively swollen U
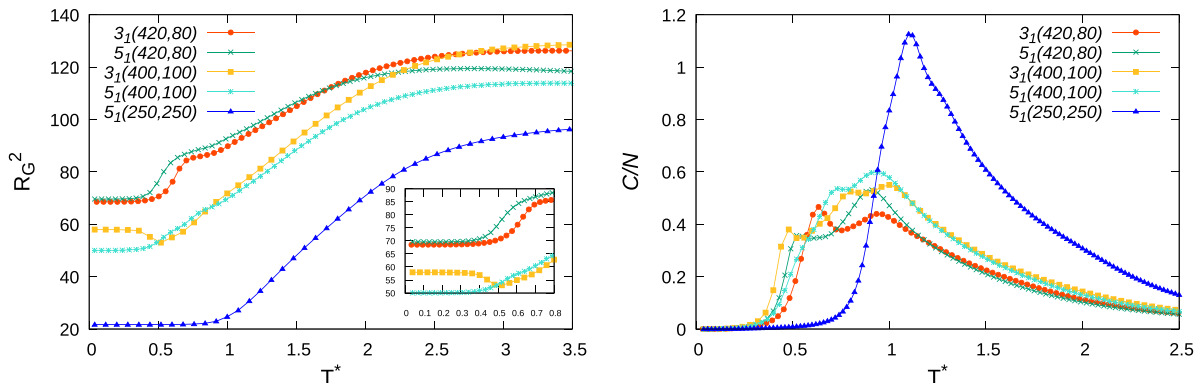

FIG. 15. Plots of the mean-square gyration radius and the specific heat capacity of a few knots with length $N = 500$ in three different monomer distributions.

phase at high temperatures. The presence of an extra peak in the specific heat capacity of longer polymers with $N_A \gg N_B$ shows the existence of an additional, intermediate I phase similarly as in proteins [79]. The I phase has been investigated with the help of several numerical experiments. Using cutoffs that increasingly restrict the energy interval until the peak of the transition from the M phase to the I phase disappears, see Fig. 8, it has been possible to establish which energies are relevant for this transition. In all cases studied here it turns out that it is sufficient to reduce the energy interval from below by approximately 10% to eliminate the peak at lower temperatures. The remaining peak can be assigned to the main expansion of the knotted copolymer ring, because it appears in coincidence with the range of temperatures in which there is a substantial increase of the gyration radius. A close inspection of the conformations at the energies that are relevant for the M and I phases has shown that these conformations are characterized by a bulk held together by the bonds between the A and B monomers, but in the I phase the tails departing from the bulk are decidedly longer than in the M phase. It is the melting of the bulk that causes the swelling of the knot leading to the U phase. A new quantity, namely the histogram $H_E(m_{AB})$ of the number m_{AB} of bonds between the A and B monomers for states with energy E, has been introduced in order to explore the energy landscape of the system and to understand why the states in the I phase are not just intermediate steps of the knot expansion on heating. It has been found that, whenever there is a double peak in the specific heat capacity, also this histogram has two peaks in the low energy spectrum, see Fig. 13. This means that states with the same energy E are characterized in the lower energy spectrum by two possible values of the number of contacts m_{AB}. The obtained data are compatible with an energy landscape of the form given in Fig. 12, in which the free energy of the system has two close minima $\bar{M}$ and $\bar{I}$, with $\bar{M}$ corresponding to the M phase and $\bar{I}$ corresponding to the I phase. The most probable value of the number m_{AB} of contacts formed by the A and B monomers depends if the conformation of the knotted copolymer is near one minimum or the other. Analyzing the histogram $H_E(m_{AB})$, it has been possible to understand why the conformations in the I phase are so stable to form a new phase. It turns out that they contain a slightly higher number of A-B bonds than states of the M phase. At low temperatures, this is sufficient to stabilize the knotted polymers against the thermal fluctuations. In correspondence with the increase of m_{AB} during the transition from the M to the I phase, the plots of the number m_{AA} has a sudden small bump, making the total energy of the conformations in the M phase lower than that of the conformations in the I phase as expected. More intermediate phases may occur in longer knots. For instance, up to three peaks have been observed in the specific heat capacity of the knot

3_1 with $N = 500$ and monomer distribution $D(400, 100)$, see Fig. 15, and knot 4_1 with $N = 300$ and monomer distribution $D(250, 50)$, see Fig. 14. Figures like Fig. 8 allow us also to estimate the fractions of energy involved in the M-I and I-U transitions.

Our investigations have also shown a strong intertwining between monomer distribution and topology. The effects of topology are visible in the plots of the gyration radius and specific heat capacity reported in Figs. 4 and 5.

Before concluding, we discuss possible improvements and directions for future research work. The simulations presented in this paper require the sampling of an extensive amount of knot conformations. Despite major improvements in the sampling procedure, that of rare events is still a problem in the case of long polymers. Some of the conformations appear after several hundred billions of trials and their inclusion extends enormously the calculation times. Moreover, in this work very short-range interactions have been considered. This is enough to study the cases of flexible knots in a good or bad solutions, but it would be interesting to add more complicated interactions. In this way, it would be possible for instance to consider also the polymer rigidity and the transition from bad to good solvents at the theta point. Work is in progress to implement in our code the backbone rigidity and the Lennard-Jones interactions. As a curiosity, in the intermediate state of the knot 4_1 with length $N = 200$ and monomer distribution $D(167, 33)$ the knot seems to be localized in the compact bulk and not in the long tail, see Fig. 9. It would be interesting to check if this remains true also in the case of longer knots or knots with different topologies.

Recently, the following articles concerning closely related subjects have been published: Refs. [40], [81], and [82].

[1] *Molecular Catenanes, Rotaxanes and Knots, a Journey through the World of Molecular Topology*, edited by J. P. Sauvage, C. Dietrich-Buchecker (Wiley-VCH Verlag, Weinheim, 1999).

[2] J. Arsuaga, J. Roca, and D. W. Sumners, Topology of Viral DNA, in *Emerging Topics in Physical Virology*, edited by

P. G Stockley and R. Twarock (Imperial College Press, London, 2010).

[3] G. Gil-Ramírez, D. A. Leigh, and A. J. Stephens, Angew. Chem. Int. Ed. **54**, 6110 (2015).

[4] J.-P. Sauvage and D. B. Amabilino, Templated synthesis of knots and ravels, in *Supramolecular Chemistry: From Molecules*

to Nanomaterials, edited by P. A. Gale and J. W. Steed (Wiley Online Library, New York, 2012).

[5] *Topological Polymer Chemistry*, edited by Y. Tezuka (World Scientific, Singapore, 2013).

[6] S. D. P. Fielden, D. A. Leigh, and S. L. Woltering, Angew. Chem. Int. Ed. **56**, 11166 (2017).

[7] M.-L. Tong and X.-M. Chen, Synthesis of coordination compounds and coordination polymers, in *Modern Inorganic Synthetic Chemistry*, edited by Ruren Xu and Yan Xu, 2nd ed. (Elsevier B. V., Amsterdam, 2017), pp 189–217.

[8] T. Stauch and A. Dreuw, Angew. Chem. Int. Ed. **55**, 811 (2016).

[9] N. Katsonis, F. Lancia, D. A. Leigh, L. Pirvu, A. Ryabchun, and F. Schaufelberger, Nat. Chem. **12**, 939 (2020).

[10] U. Tkalec, M. Ravnik, S. Čopar, S. Žumer, and I. Muševič, Science **333**, 62 (2011).

[11] F. Bosia, E. Lepore, N. T. Alvarez, P. Miller, V. Shanov, and N. M. Pugno, Carbon **102**, 116 (2016).

[12] L. H. Kauffman, *Knots and Physics*, Series on Knots and Everything: Vol. 1, 3rd ed. (World Scientific, Singapore, 2001).

[13] L. H. Kauffman and S. Lambropoulou, Classifying and applying rational knots and rational tangles, in *Physical Knots: Knotting, Linking, and Folding Geometric Objects in $\mathbb{R}^3$*, edited by J. A. Calvo, K. C. Millett, and E. J. Rawdon, Contemporary Mathematics AMS Series Vol. 304 (American Mathematical Society, Providence, RI, 2002), pp. 223–258.

[14] A. Y. Grosberg, Polym. Sci. Ser. A **51**, 70 (2009).

[15] A. Suma, A. Rosa, and C. Micheletti, ACS Macro Lett. **4**, 1420 (2015).

[16] L. Tubiana, E. Orlandini, and C. Micheletti, Prog. Theor. Phys. Suppl. **191**, 192 (2011).

[17] A. L. Kholodenko and T. A. Vilgis, Phys. Rep. **298**, 251 (1998).

[18] S. Majumder, M. Marenz, S. Paul, and W. Janke, Macromolecules **54**, 5321 (2021).

[19] I. Chubak, C. N. Likos, and J. Smrek, J. Molecular Phys. **119**, e1883140 (2021).

[20] R. Kumar Sharma, I. Agrawal, L. Dai *et al.*, Nat. Commun. **10**, 4473 (2019).

[21] D. Meluzzi, D. E. Smith, and G. Arya, Annu. Rev. Biophys. **39**, 349 (2010).

[22] C. Micheletti, D. Marenduzzo, and E. Orlandini, Phys. Rep. **504**, 1 (2011).

[23] A. R. Klotz, B. W. Soh, and P. S. Doyle, Phys. Rev. Lett. **120**, 188003 (2018).

[24] F. Wang and D. P. Landau, Phys. Rev. Lett. **86**, 2050 (2001).

[25] E. Orlandini, M. Baiesi, and F. Zonta, Macromolecules **49**, 4656 (2016).

[26] L. Dai and P. S. Doyle, Polymers **9**, 57 (2017).

[27] A. Yu. Grosberg and A. R. Khokhlov, *Giant Molecules: Here, There, and Everywhere*, 2nd ed. (World Scientific, Singapore, 2011).

[28] C. Vlahos, N. Hadjichristidis, M. K. Kosmas, A. M. Rubio, and J. J. Freire, Macromolecules **28**, 6854 (1995).

[29] J. F. Marko, Macromolecules **26**, 1442 (1993).

[30] A. Weyersberg and T. A. Vilgis, Phys. Rev. E **48**, 377 (1993).

[31] R. Hołyst and T. A. Vilgis, Macromol. Theory Simul. **5**, 573 (1996).

[32] K. Huber, Macromolecules **21**, 1305 (1988).

[33] R. H. Abdolvahab, M. R. Ejtehadi, and R. Metzler, Phys. Rev. E **83**, 011902 (2011).

[34] M. P. Taylor, W. Paul, and K. Binder, J. Chem. Phys. **131**, 114907 (2009).

[35] S. E. Kudaibergenov and O. Okay, Polym. Adv. Technol. **32**, 2639 (2021).

[36] N. A. Volkov, P. N. Vorontsov-Velyaminov, and A. P. Lyubartsev, Phys. Rev. E **75**, 016705 (2007).

[37] F. Ferrari, Block copolymer knots, arXiv:1603.08972 [cond-mat.soft].

[38] P. G. Dommersnes, Y. Kantor, and M. Kardar, Phys. Rev. E **66**, 031802 (2002).

[39] A. Tagliabue, C. Micheletti, and M. Mella, ACS Macro Lett. **10**, 1365 (2021).

[40] A. Tagliabue, C. Micheletti, and M. Mella, Macromolecules **55**, 10761 (2022).

[41] S. Najafi, R. Potestio, PLoS ONE **10**, e0132132 (2015).

[42] A. Kuriata and A. Sikorski, Macromolec. Theory Simul. **27**, 1700089 (2018).

[43] H. Benahmed, Chin. J. Phys. **73**, 256 (2021).

[44] T. Herschberg, J.-M. Y. Carrillo, B. G. Sumpter, E. Panagiotou, and R. Kumar, Macromolecules **54**, 7492 (2021).

[45] C. Cardelli, L. Tubiana, V. Bianco, F. Nerattini, C. Dellago, and I. Coluzza, Macromolecules **51**, 8346 (2018).

[46] K. A. Dill, S. Bromberg, K. Yue, K. M. Fiebig, D. P. Yee, P. D. Thomas, and H. S. Chan, *Principles of Protein Folding—A Perspective from Simple Exact Models* (Cambridge University Press, Cambridge, UK, 1995).

[47] See also Refs. [60,61] for investigations of HP models using the Wang-Landau algorithm.

[48] P. N. Vorontsov-Velyaminov, N. A. Volkov, and A. A. Yurchenko, J. Phys. A: Math. Gen. **37**, 1573 (2004).

[49] A. Swetnam, C. Brett, and M. P. Allen, Phys. Rev. E **85**, 031804 (2012).

[50] W. Wang, Y. Li, and Z. Lu, Sci. China Chem. **58**, 1471 (2015).

[51] V. Katritch, J. Bednar, D. Michoud *et al.*, Nature London **384**, 142 (1996).

[52] S. R. Quake, Phys. Rev. Lett. **73**, 3317 (1994).

[53] The probability of states of given energy to occur during a simulation may be computed using the density of states, see Sec. II.

[54] Y. Iba, N. Saito, and A. Kitajima, Ann. Inst. Stat. Math. **66**, 611 (2014).

[55] E. E. Borrero and C. Dellago, Jour. Chem. Phys. **133**, 134112 (2010).

[56] Y. W. Li, T. Vogel, T. Wüst, and D. P. Landau, J. Phys.: Conf. Ser. **510**, 012012 (2014).

[57] Y. Zhao and F. Ferrari, Physica A **486**, 44 (2017).

[58] F. Ferrari and Y. Zhao, Rev. Math. Phys. **33**, 2150005 (2021).

[59] J. Jeon and A. V. Dobrynin, J. Phys. Chem. B **110**, 24652 (2006).

[60] T. Wüst and D. P. Landau, J. Chem. Phys. **137**, 064903 (2012).

[61] T. Wüst, D. Reith, and P. Virnau, Phys. Rev. Lett. **114**, 028102 (2015).

[62] Y. Zhao and F. Ferrari, J. Stat. Mech. (2013) P10010.

[63] Y. Burak, G. Ariel, and D. Andelman, Curr. Opin. Colloid Interface Sci. **9**, 53 (2004).

[64] C. Holm, J. F. Joanny, K. Kremer, R. R. Netz, P. Reineker, C. Seidel, T. A. Vilgis, and R. G. Winkler, Adv. Polym. Sci. **166**, 67 (2004).

[65] E. J. Janse van Rensburg and A. Rechnitzer, J. Stat. Mech. (2011) P09008.

[66] R. Scharein *et al.*, J. Phys. A: Math. Theor. **42**, 475006 (2009).

[67] T. Kennedy, J. Stat. Phys. **106**, 407 (2002).

[68] Y. Zhao and F. Ferrari, J. Stat. Mech. (2012) P11022.

[69] N. Madras, A. Orlistsky, and L. A. Shepp, J. Stat. Phys. **58**, 159 (1990).

[70] M. Ozmaian and D. E. Makarov, PLoS ONE **18**, e0287200 (2023).

[71] The differences from knot to knot in the plots of R_G^2 and C/N cannot be attributed to statistical errors: Every simulation has been repeated several times changing the starting seed and no significant changes have been observed.

[72] G. M. Grason *et al.*, Phys. Rev. Lett. **91**, 058304 (2003).

[73] E. Orlandini, A. L. Stella, and C. Vanderzande, Phys. Rev. E **68**, 031804 (2003).

[74] L. Tubiana, G. Polles, E. Orlandini, and C. Micheletti, Kymo-knot: A web server and software package to identify and locate knots in trajectories of linear or circular polymers, Eur. Phys. J. E **41**, 72 (2018).

[75] F. Rampf, W. Paul, and K. Binder, Europhys. Lett. **70**, 628 (2005).

[76] T. Vogel, M. Bachmann, and W. Janke, Phys. Rev. E **76**, 061803 (2007).

[77] M. Bachmann and W. Janke, Phys. Rev. Lett. **91**, 208105 (2003).

[78] Y.-H. Hsieh, C.-N. Chen, and C.-K. Hu, EPJ Web Conf. **108**, 01005 (2016).

[79] P. L. Privalov, J. Mol. Biol. **258**, 707 (1996).

[80] N. G. Fytas and P. E. Theodorakis, J. Phys.: Condens. Matter **23**, 235106 (2011).

[81] K. Hagita, T. Murashima, N. Sakata, K. Shimokawa, T. Deguchi, E. Uehara, and S. Fujiwara, Macromolecules **56**, 15 (2023).

[82] A. Kuriata and A. Sikorski, J. Mol. Liq. **379**, 121664 (2023).